Characterisation of putative retrotrapezoid nucleus (RTN) chemoreceptor neurons in the adult human brainstem

Yazhou Liu[1], Rita Machaalani[2], Irit Markus[1], Claire E. Shepherd*[1,3], Natasha N. Kumar*[1]

[1]Faculty of Medicine and Health, The University of New South Wales, NSW, 2052, Australia

[2] Sydney Medical School, Faculty of Medicine and Health, University of Sydney, NSW, 2006, Australia

[3] Neuroscience Research Australia, Barker Street, NSW, Australia.

Corresponding author: Natasha N Kumar (natasha.kumar@unsw.edu.au)

Authors ORCIDS:

Yazhou Liu: 0000-0002-2096-4064

Natasha Kumar: 0000-0003-4712-8792

Rita Machaalani: 0000-0002-7675-1121

Irit Markus: None

Claire Shepherd: 0000-0002-0399-3218

*Co-senior authors

Abstract

The retrotrapezoid nucleus of rodents (RTN) is located ventral to the facial motor nucleus (7N) and consists of acid-sensitive neurons that activate breathing and mediate the central component of the ventilatory response to hypercapnia (HCVR). In rats and mice RTN neurons can be histologically identified by the presence of paired-like homeobox 2B positive nuclei (Phox2b+) and the absence of cytoplasmic choline acetyltransferase (ChAT-) and tyrosine hydroxylase (TH-). Furthermore, up to 50% of rodent RTN neurons synthesise galanin, and 100% express pituitary adenylate cyclase activating polypeptide (PACAP) and neuromedin B (NMB). The human RTN (hRTN) has been tentatively identified in two infant studies and one adult study, but it was not mapped. This study aimed to map the location and cytoarchitecture of the adult hRTN and compare the findings to the literature of rodents, macaques and human infants. Formalin-fixed, paraffin-embedded tissue blocks from two adult cases, spanning the medulla-pons, were serially sectioned (10µm thick) and every four in thirty sections were immunohistochemically stained with ChAT, and double stained Phox2b/TH, Phox2b/galanin and Phox2b/PACAP. Immunostained sections were scanned and analysed using QuPath software. hRTN neurons were identified by their Phox2b positive (Phox2b+) nucleus and negative cytoplasm for TH and ChAT (Phox2b+/TH-/ChAT-). Such neurons were identified ventral to 7N, lateral to the superior olive, overlapped with the C1 catecholaminergic population and extended rostrocaudally from Obex +13 mm to Obex +17 mm. hRTN neurons comprised 90% of Phox2b+ neurons in the parafacial area, totaling around 5000 bilaterally, and were surrounded by numerous TH-ir fibers. Galanin and PACAP immunoreactivity was identified in 43% and 38% of Phox2b+ parafacial neurons, respectively. This is the first study to characterise and quantitatively map the adult human RTN using a series of neurochemical markers.

Keywords

Human RTN, Phox2b, chemoreception, immunohistochemistry, galanin, PACAP

Abbreviations

4V, 4th ventricle; 6N, abducens nucleus; 6n, abducens nerve; 7N, facial motor nucleus; 7n, facial nerve; 8n, vestibulocochlear nerve; Biotin-SP-conjugated, biotin-succinimidyl ester conjugated; C1, C1 adrenergic neurons; CCHS, congenital hypoventilation syndrome; ChAT, choline acetyltransferase; CO_2, carbon dioxide; D, dorsal; DAB, 3,3'-diaminobenzidine; DPX, dibutylphthalate polystyrene xylene; FFPE, formalin-fixed, paraffin-embedded; H_2O_2, hydrogen peroxide; H&E, hematoxylin & eosin; hRTN, human retrotrapezoid nucleus; HIER, heat-induced epitope retrieval; icp, inferior cerebellar peduncle; IC, inferior colliculus; IF, immunofluorescence; IgG, immunoglobulin G; IHC, immunohistochemistry; IO, inferior olive; IOP, inferior olive, principal nucleus; IRt, intermediate reticular nucleus; IS, inferior salivatory nucleus; ISH, in situ hybridisation; mcp, medial cerebellar peduncle; ml, medial lemniscus; MSO, medial superior olive; NDS, normal donkey serum; NK1R,

neurokinin-1 receptor; NMB, neuromedin B; NTS, nucleus of the solitary tract; PACAP, pituitary adenylate cyclase activating polypeptide; PBS, phosphate-buffered saline; PCRt, parvocellular reticular nucleus; PCRtA, parvocellular reticular nucleus, alpha; Phox2b, paired-like homeobox 2B; ppGal, preprogalanin; Pn, pontine nuclei; py, pyramidal tract; R, rostral; RNA, ribonucleic acid; ROI, regions of interest; RRID, Research Resource Identifier; RTN, retrotrapezoid nucleus; SC, superior colliculus; SEM, standard error of the mean; SIDS, Sudden Infant Death Syndrome; SLC17A6, solute carrier family 17 member A6 (vesicular glutamate transporter 2 gene); SO, superior olive; Sp5, spinal trigeminal nucleus; Sp5I, spinal trigeminal nucleus, interpolar part; Sp5O, spinal trigeminal nucleus, oral part; sp5, spinal trigeminal tract, nerve; TBS, Tris-buffered saline; TH, tyrosine hydroxylase; V, ventral; vGlut2, vesicular glutamate transporter 2; VRC, ventral respiratory column; WB, Western blotting.

Introduction

In mammals, breathing depends on the generation and regulation of respiratory rhythm, which is controlled by the central respiratory nuclei and neural network in the brainstem (Ikeda et al., 2017). Central respiratory chemoreceptors are clusters of cells in the lower brainstem respiratory network which regulate breathing stimulated by carbon dioxide (CO_2) or its proxy, protons (H^+) (Guyenet and Bayliss, 2015, Wang et al., 2013, Ikeda et al., 2017, Ramirez et al., 2018, Barnett et al., 2017, Mulkey and Wenker, 2011). Acid sensing chemoreceptor neurons in the retrotrapezoid nucleus (RTN) (Guyenet and Bayliss, 2015, Guyenet and Bayliss, 2022) project to the ventral respiratory column (VRC) which drives the central respiratory chemoreflex response (Guyenet et al., 2019). Impaired central respiratory chemoreception results in an impaired hypercapnic ventilatory response, as occurs in congenital hypoventilation syndrome (CCHS) and central sleep apnea (Kasi et al., 2018, Meylemans et al., 2021, Degl'Innocenti et al., 2018, Amiel et al., 2009, Dereli et al., 2019).

The RTN comprises about 2000 neurons in the rat, and 800 neurons in mice (Takakura et al., 2008, Guyenet and Bayliss, 2015, Shi et al., 2017). Phox2b is the most widely recognised biomarker for RTN chemoreceptors, and changes in its expression are regarded as an indicator of RTN chemoreceptor dysfunction associated with various central respiratory disorders in both rodents and humans (Amiel et al., 2009, Goridis and Brunet, 2010, Dubreuil et al., 2009, Meylemans et al., 2021, Lavezzi et al., 2012). In addition to Phox2b, alterations in neuropeptides, such as galanin and PACAP, are important for regulation of central chemoreception in the RTN. In rodents, galanin is expressed in approximately 50% of RTN neurons (Stornetta et al., 2009) and the pre Botzinger complex receives glutamatergic innervation from galaninergic RTN neurons (Bochorishvili et al., 2012, Dereli et al., 2024). Long term hypercapnia induces an increase in preprogalanin (ppGal)

expression in the RTN (Dereli et al., 2019) and microinjection of galanin into the VRC, specifically in the PreBotzinger and Botzinger complexes, impairs the chemoreflex response to hypercapnia (Abbott et al., 2009). In neonatal mice, PACAP is expressed in 100% of RTN chemoreceptor neurons and the deletion of PACAP in RTN neurons leads to elevated incidence of apneas and reduced respiratory responses to CO_2 stimulation in the postnatal period (Shi et al., 2021). Although PACAP expression in the human brainstem has been studied (Huang et al., 2017), the RTN was not investigated due to the lack of knowledge regarding its precise location.

To date, four studies have investigated the location of the RTN in primates; 1 in monkeys and 3 in humans (Table 1). Levy and colleagues aimed to identify Phox2b mRNA in formalin fixed and paraffin embedded (FFPE) adult human brainstem, but it failed to be detected and as such, the data was on a population of preprogalanin (ppGal+)/ Solute Carrier Family 17 Member A6 (SLC17A6)+ mRNA containing neurons in the parafacial region (Levy et al., 2021). The other two studies were conducted on FFPE tissue from foetuses or infants (Rudzinski and Kapur, 2010, Lavezzi et al., 2012). (Rudzinski and Kapur, 2010, Lavezzi et al., 2012)Rudzinski and Kapur (2010), described the putative human RTN (hRTN) population as a discontinuous cluster of small- to medium-sized Phox2b positive/ Neurokinin 1 receptor positive/Tyrosine hydroxylase negative (Phox2b+/NK1R+/TH-) neurons situated ventral to the facial motor nucleus (7N) and lateral to the superior olivary nucleus (SO) spanning from the caudal pons to the rostral medulla (Rudzinski and Kapur, 2010). Lavezzi et al (2012) described the RTN as a cluster of Phox2b+ neurons situated between the 7N and SO in the caudal pons (Lavezzi et al., 2012). While both infant studies sought to characterise the hRTN, they were restricted by limited tissue sampling and differences in staining patterns (Table 1).

Since the RTN has not been systematically mapped using Phox2b in the human brainstem, our overall study goal was to fill this research gap. This immunohistochemical study used post-mortem formalin-fixed, paraffin-embedded tissue from 2 adult humans to: 1) characterize Phox2b immunohistochemical staining in the RTN region, specifically ventral to 7N, 2) establish the neurochemical signature of hRTN neurons and quantify these neurons, 3) establish the neuroanatomical location and dimensions of the hRTN neuronal population in relation to 7N and C1 catecholaminergic neurons, 4) identify the proportion of parafacial Phox2b+ neurons expressing the neuropeptides galanin and PACAP, and 5) describe the morphological features (size and density) of parafacial Phox2b+ neurons. Our findings provide valuable insights for investigations into Phox2b-associated disorders, particularly those involving respiratory and autonomic dysfunction including CCHS and sleep apnea.

Methods

Human Tissue Selection

Post-mortem, formalin-fixed brainstem tissue specimens from two adult human cases (76-year-old female, and 87-year-old male; Supplementary Table 1), were sourced from the Sydney Brain Bank through regional brain donor programs in Sydney, Australia. In adherence to the case inclusion criteria, the post-mortem samples were acquired from asymptomatic individuals exhibiting solely age-related brain changes and devoid of significant neuropathology. Notably, exclusion criteria also included documented respiratory drive disorders, post-mortem delays exceeding 72 hours and tissue formalin fixation exceeding a ten-year period. The demographic and autopsy characteristics of these two cases are presented in Supplementary Table 1.

Brainstem tissue blocks spanning from the rostral medulla oblongata (Obex +12 mm) to the caudal pons (Obex +18 mm) were selected (Figure 1), as this region is known to contain the 7N and is expected to include the hRTN. The selected Obex range was guided by Paxinos' human brain atlas (Paxinos et al., 2020) and anatomical features identified in Hematoxylin & Eosin (H&E)-stained sections).

Tissue sectioning

Ten-micron, serial sections were cut from formalin-fixed, paraffin-embedded tissue blocks (2-3 mm thick transverse oriented brainstem blocks) using a rotary microtome. We collected approximately 700 sections per case, extending rostrocaudally from Obex +18 mm to Obex +12 mm). One in every thirty serial sections (300 µm apart) was stained with Hematoxylin & Eosin (H&E), to obtain representative sections containing the 7N.

Once the full extent of the 7N had been mapped in H&E sections, four of every thirty serial sections were selected for immunohistochemistry, and stained with antibodies against ChAT , Phox2b+TH, Phox2b+PACAP and Phox2b+galanin, respectively (Table 2). As a result, each identically stained section was spaced 300µm apart (Supplementary Table 2).

Immunohistochemistry (IHC) Protocol for Human FFPE Brain Tissue

The IHC protocol steps were based on our previously reported method (Huang et al., 2017), however optimisation for Phox2b immunohistochemistry was required (detailed in Supplementary Material 1). Following deparaffinisation and rehydration, antigen retrieval was performed using heat-induced epitope retrieval (HIER) with Target Retrieval Solution (Citrate pH 6, #S2369, Agilent DAKO) in a HIER antigen retrieval chamber (Decloaking Chamber™ NxGen, #DC2012-220V,

Borcare Medical) for 15 minutes. Endogenous peroxidase activity was quenched with 3% hydrogen peroxide (H_2O_2)/0.1 M Phosphate Buffered Saline (PBS) for 15 minutes, followed by washes in 1×PBS and Tris Buffered Saline (1×TBS) for 10 minutes each. Sections were then blocked for 2-hours in 10% normal donkey serum (NDS) in TBS with 0.3% Tween 20.

Tissue was then incubated overnight with one primary antibody, and subsequently for 2-hours in biotinylated secondary antibody, diluted in 2% NDS in TBS with 0.1% Tween 20. After washing in TBS, sections were incubated with avidin/biotin complex (Vectastain Elite ABC HRP Kit, #PK-6100, Vector Laboratories) for 40 minutes to amplify the reaction. Visualisation was achieved using 3,3'-diaminobenzidine (DAB) or DAB/Nickel (DAB Substrate Kit, #SK-4100, Vector Laboratories).

For dual IHC staining (Phox2b+TH, Phox2b+PACAP, or Phox2b+galanin), Phox2b was first detected using DAB with nickel enhancement (black). In the sequential round of immunohistochemistry assay, the tissue was incubated with a primary antibody against TH (chicken anti-TH), PACAP (rabbit anti-PACAP), or galanin (rabbit anti-galanin) (Table 2), followed by a corresponding secondary antibody and DAB (brown) detection. After dehydration and clearing, sections were mounted using dibutylphthalate polystyrene xylene (DPX), and coverslipped. Antibody details and concentrations are listed in Table 2.

Microscopy and Imaging

Immunostained slides were digitised using an Aperio Digital Pathology Slide Scanner (Aperio AT2, Leica BioSystems) at 20× magnification. The scanned files were viewed using QuPath Software (Version 0.2.3) (Bankhead et al., 2017). Coronal hemi-sections approximating from Obex +12 mm to Obex +18 mm were assessed. Anatomical landmarks such as the Sp5O, the 7N and the facial nerve were located according to a human brainstem atlas (Paxinos et al., 2020) and used to identify various rostrocaudal levels relative to Obex (Figure 1 b & c).

Quantitative analyses

The cell diameter, and area of the cell soma and nucleus of RTN neurons, were measured using QuPath tools (See details in Supplementary Material 2). This data was collated using Microsoft Excel v14.0 (2010, Microsoft, USA), and exported into GraphPad Prism (Version 9, CA, USA).

Neurons with the following neurochemical signatures were counted:

1- Parafacial neurons, located ventrolateral to the 7N, as:
    a. RTN neurons: Phox2b+ nucleus, TH- and ChAT- cytoplasm,
    b. PACAP and Phox2b double-labelled (Phox2b+ nucleus, PACAP+ cytoplasm),
    c. Galanin and Phox2b double-labelled (Phox2b+ nucleus, galanin+ cytoplasm),

2- 7N neurons as ChAT+ cytoplasm, and

3- C1 neurons as TH+ cytoplasm

Number of RTN neurons was calculated applying the formula derived from (Abercrombie, 1946):

RTN Cell Count (N) = $RTN\ hemisection\ cell\ count\ (n) \times \frac{T}{T+D} \times 2 \times 30$

N, actual RTN cell count; n, RTN cell count/hemi-section; T, thickness of the section; D, average diameter of the cell.

Data from the 2 adult cases was averaged and presented as mean ± SEM. No statistical analysis was performed due to the study being an anatomical description of the hRTN, without comparison between a control and experimental group.

Results

Immunoreactive pattern of staining

The subcellular localisation of labeling for each primary antibody was as expected (Figure 2). ChAT, TH, PACAP and galanin immunoreactivity were observed in the cytoplasm and fibers of neurons, while Phox2b immunoreactivity was confined to the nucleus of neurons (Figure 2).

For Phox2b, positive staining was subcategorised as either strong or weak (Supplementary Figure 1), and counting was performed separately for each category before combining the results (rationale and detailed in Supplementary Material 3).

Neurochemical signature of putative hRTN neurons

Identification of RTN neurons according to their biochemical signature of Phox2b+ nucleus, TH-/ChAT- cytoplasm, was clearly discernable from neighboring 7N (ChAT+) and overlapping C1 (TH+) neurons (Figure 3). TH+ fibers coursed through the RTN region (Figure 3a). In a high magnification image (Figure 3b), the TH-positive axons were clearly delineated, and TH+ boutons made close appositions with RTN neurons. The subcellular labelling of these neurochemical markers in the RTN and nearby nuclei (7N and C1) is documented in Table 3. A few Phox2b+TH- neurons were also detected in spinal trigeminal nucleus, oral part (Sp5O) (Figure 3c), intermediate reticular nucleus (IRt) and parvocellular reticular nucleus (PCRt) (Figure 3d).

Phox2b+ parafacial neurons are immunoreactive for galanin and PACAP

Although TH immunohistochemistry was not performed in combination with Phox2b/PACAP or Phox2b/galanin labelling, our quantitative data show that the majority of Phox2b-immunoreactive neurons located ventral to the facial nucleus (7N) are devoid of TH immunoreactivity. This strongly suggests that these neurons are part of the RTN population. Therefore, in this context, we confidently identified RTN neurons based on their Phox2b expression and anatomical location within the parafacial region. Based on the double labelling for Phox2b and galanin as well as the double labelling for Phox2b and PACAP, a total of 5295 Phox2b+ parafacial neurons were counted (Table 4).

Galanin immunoreactivity was detected in the soma and dendrites of Phox2b+ parafacial neurons (Figure 4a-c) and represented 43% of the total Phox2b+ population (2262 galanin+/Phox2b+ neurons out of 5296 Phox2b+ parafacial neurons) (n=2, with 14 sections counted per case) (Supplementary Table 3). Similarly, PACAP immunoreactivity was confined to the cell soma and dendrites of 39.5% Phox2b+ parafacial neurons (2090 PACAP+Phox2b+ parafacial neurons out of 5296 Phox2b+ parafacial neurons, Figure 4d-f) of Phox2b+ parafacial neurons PACAP+ (Supplementary Table 3).

Anatomical characteristics of the hRTN based on the distribution of Phox2b+/TH- neurons

Putative hRTN neurons were located ventral and ventrolateral to the 7N, lateral to the SO, dorsomedial to the pontomedullary junction, medial to the Sp5O, spinal trigeminal tract (sp5) and the facial nerve, and overlapping with C1 catecholaminergic neurons (Figure 3).

RTN neurons were found from Obex +13 mm to Obex +17 mm (Figure 5 and 6) of the medulla oblongata. At caudal levels, Obex +13 mm to Obex +13.8 mm-, the RTN neurons were sparsely distributed (Figure 5 and Figure 6a). By contrast, within the range of +13.8 mm to +14.8 mm, RTN neurons formed a distinct and prominent cluster (Figure 5), indicated by a concentrated presence of Phox2b+/TH- neurons. More rostrally, (+14.8 mm to +16.8 mm), the RTN neurons were again more sparsely distributed, devoid of a distinct cluster (Figure 5 and Figure 6c). Anatomically, rostral RTN neurons were distributed medial to the facial nerve, ventrolateral to the 7N, dorsal to the ventral surface of the medulla and lateral to the SO (Figure 5).

Morphology of hRTN neurons

The soma of RTN neurons was typically round, or fusiform, with one or two dendrites extending in various directions (Figure 4). RTN neurons were significantly smaller in size compared to 7N and C1 neurons, with an average soma area of 309.9 ± 61.8 μm^2 (n=241 cells), and an average nucleus area of 69.0±23.3 (Table 3).

Quantification of hRTN neurons

Based on Phox2b+/TH- staining, the number of putative RTN neurons ranged from 5 to 65 per hemi-section, with a peak observed between Obex +14.0 mm and +14.3 mm (Figure 7a). Considering both

weak and strong stained Phox2b, the total number of RTN neurons was 5102 ± 280.5 (n=2, Table 4), spanning 4 mm in rostrocaudal length (Figure 7a).

The rostrocaudal distribution of galanin+/Phox2b+ and PACAP+/Phox2b+ parafacial neurons followed the same trend, showing a peak in counts at Obex 14 mm and spanning 4mm in rostrocaudal length (Figure 7 b and c). From these double stained sections, a total of 5296 Phox2b+ parafacial neurons were counted (Table 4). The galanin population was 43% of the total Phox2b+ population while PACAP was 39.5% (Table 4).

Discussion

This study provides a comprehensive characterisation of the adult human RTN using histological and neuroanatomical means. Leveraging previous reports from infant and rodent studies, we identified a large cluster of Phox2b+/TH- neurons ventral to the 7N, aligning with the expected location of the RTN. We present the first in-depth analysis of the rostrocaudal distribution of Phox2b+ RTN neurons in the adult human brainstem, detailing cell counts, morphological parameters and neuropeptide expression (galanin and PACAP), both relevant to respiratory function. We also demonstrate puncta from TH+ fibers (catecholaminergic neurons) apposing RTN neurons. These findings establish a crucial baseline of the healthy aged adult human RTN, which is essential for understanding potential pathological alterations, such as neuronal loss, morphological changes or respiratory relevant neuropeptide deficits, in respiratory and neurological disorders.

Adult human RTN neurons are Phox2b positive and subsets express galanin and PACAP immunoreactivity

In this study, the human adult RTN was identified using the histological criteria for identification of RTN neurons in adult rodents; namely, parafacial neurons that express the transcription factor Phox2b and are devoid of TH and ChAT immunoreactivity (Guyenet and Bayliss, 2022). Our data identifies a highly circumscribed cluster of Phox2b neurons in the adult human RTN, in agreement with findings in infants The 43% galanin+ neurons in the total Phox2b+ parafacial neuronal population within the RTN region, closely aligns with findings from adult rat studies (Stornetta et al., 2009). Furthermore,

the quantification of galaninergic neurons in our study of 2262 is comparable to that reported in the macaque of around 2400 galaninergic neurons within the RTN (Levy et al., 2019). (Levy et al., 2021)

The location of hRTN neurons in the adult is highly consistent with the distribution reported in human infants and other species

In this study, the spatial distribution of adult hRTN neurons aligns well with findings from rodents, non-human primates, and human infants (Levy et al., 2019, Levy et al., 2021, Lavezzi et al., 2012, Rudzinski and Kapur, 2010, Shi et al., 2017). Dorsoventrally, the RTN neurons are situated dorsal to the pontomedullary junction, lateral to the superior olive, and ventrolateral to the 7N. Rostrocaudally, hRTN neurons extended from Obex +13mm to Obex +17 mm in the brainstem. A previous study in adult humans identified putative RTN neurons using ppGal and SLC17A6 (vGlut2) mRNA expression as markers. That study reported galanin+VGlut2+ putative RTN neurons extending from Obex +14 mm to Obex +17 mm (Levy et al., 2021). This shorter rostrocaudal extent observed may have led to an underestimation of RTN neuron numbers, potentially due to discrepancies between versions of the human brainstem atlas. Notably, the Paxinos 2012 atlas (used by (Levy et al., 2021)), describes the facial motor nucleus as is 3 mm long whilst the updated Paxinos 2020 reports a 4 mm in rostrocaudal length, consistent with our current findings. Nevertheless, both our findings and Levy's demonstrate close proximity between the RTN and 7N throughout their rostrocaudal extent. This consistency underscores the reliability of the findings.

Another key difference between our study and Levy's (Levy et al., 2021) is the biomarkers used to identify RTN neurons. While our study successfully detected Phox2b-ir, Levy et al. relied on vGlut2 and ppGal co-expression, due to failure in detecting Phox2b signal (Levy et al., 2021). However, the non-galaninergic RTN neurons were not defined (Levy et al., 2021). Since, galanin expression is reported in 40% to 60% RTN neurons in rodents (Shi et al., 2017, Stornetta et al., 2009) and 43% in our findings. Therefore, using ppGal and vGlut2 as neurochemical markers to label RTN can lead to underestimation of RTN neurons.

In rodents, neuromedin B (NMB), is also considered to be specific for RTN chemoreceptors (Souza et al., 2020, Shi et al., 2017), but this is not the case in humans. In (Levy et al., 2021), NMB+ neurons were located dorsomedial to the 7N (Levy et al., 2021). This finding is in conflict with rodent macaque and human infant human studies which described putative hRTN ventral to the 7N (Lavezzi et al., 2012, Rudzinski and Kapur, 2010). They concluded that their NMB+ labelling dorsal to 7N but not ventral to 7N questions its reliability as a biomarker of hRTN neurons Our dataset represents the most complete count of RTN neurons to date including both galanin+ and galanin- RTN neurons.

The adult human contains more RTN neurons than adult rodents and macaque

We identified approximately 5000 Phox2b+TH- neurons within the putative hRTN, a count significantly higher than the approximately 980 Phox2b+ neurons reported in human infants (Lavezzi et al., 2012). The discrepancy may be related to differences in immunohistochemistry protocol or success, or due to the exclusion of "weakly stained" Phox2b+ neurons from the RTN population in analyses (Lavezzi et al., 2012, Levy et al., 2019). To determine whether excluding the weakly stained Phox2b+ RTN neurons explains the discrepancy, our stratification of counts indicated an average of 2530 strongly stained Phox2b neurons per case bilaterally, which is still significantly greater than the 980 strongly stained Phox2b RTN neurons reported by Lavezzi et al. Lavezzi et al., 2012. This discrepancy is probably not due to variability in RTN neuronal numbers across different developmental stages, since the number of RTN neurons in mice does not change from the late prenatal period to adulthood (600-700 cells). A direct comparison would require using the same tissue preservation method, immunohistochemical techniques and antigen retrieval. Interestingly, the female adult case had a 29% greater RTN number than the male adult case in our study. This suggests a possibility of gender difference in RTN development or Phox2b expression, although study on a greater number of cases is required before any conclusion can be made.

The RTN contains approximately 2000 neurons in rats (Stornetta et al., 2009, Takakura et al., 2008), 700 in mice (Lazarenko et al., 2009) and 2400 galaninergic RTN neurons in macaques (Levy et al., 2019). Our findings suggest a larger RTN population in the human compared with other species.

Whilst variability across species and developmental stages may account for differences in RTN neuronal counts and location, the discrepancies between our study and previous human studies in the total RTN cell count could also be attributed to methodological differences. Some studies did not assess serial sections and instead estimated total cell count based on the analysis of just 1-2 sections per case (Lavezzi et al., 2012). Differences in how the rostrocaudal length of the RTN region is delineated in reference atlases could also explain discrepancies between human studies (Paxinos, 2012, Paxinos et al., 2020).

C1-RTN circuit and its role in breathing control: evidence of neuronal interactions

In this study, we show that the TH+ presumptive C1 neurons are intermingled with RTN neurons, and we demonstrated close appositions between TH+ terminals and RTN neurons. Rodent studies have demonstrated that the RTN region is abundant with PNMT-ir terminals (Rosin et al., 2006)) and vigorously activated by adrenaline via α1 adrenoceptors (Oliveira et al., 2016). Furthermore, a recent optogenetic study in conscious rats demonstrated that selective photo-stimulation of C1 neurons produces effects on breathing frequency and amplitude similar to those observed with RTN photo-stimulation (Souza et al., 2020). Taken together, this suggests that the C1-RTN circuit plays a role in the central control of breathing. Therefore, it is possible that hRTN neurons receive projections from C1 catecholaminergic neurons, however, further studies are needed to determine the origin of the TH+ axons and boutons apposing hRTN neurons.

Factors affecting RTN neuronal counts and future research directions

The RTN neuronal cell count may be influenced by several factors. First, the neurochemical signature used to define RTN neurons could inadvertently include Phox2b+/TH- PCRt, IRt or Sp5O neurons located in the region dorsal and medial to 7N (Figure 4d), However these were excluded from hRTN because their distribution was anatomically discontinuous from the RTN cluster. Secondly, although this study identified hRTN neurons based on the neurochemical signature established in rodent functional studies (Lazarenko et al., 2009), further research is needed to confirm that hRTN neurons are indeed chemosensory (Shi et al., 2017). Third, we have reported RTN neuron counts in older

adults, and it is uncertain whether Phox2b+ neurons undergo age-related degeneration. If such degeneration occurs, our quantitative results may underestimate the number of Phox2b+ RTN neurons in young adults. Finally, although this study was limited by a small sample size, a key strength lies in our thorough analysis of the entire length of the RTN (14 sections per case, spanning 4mm rostrocaudally), rather than focussing on a single plane as is common in studies using post-mortem human brain tissue. A further strength is the consistent rostral-caudal distribution and the quantified peaks of RTN neurons observed across the two cases. Future studies with a larger sample size are needed to evaluate changes in this neuronal population with age, sex and with disease; this will strengthen the robustness and generalisability of our findings. Our study lays the groundwork for these future investigations and for future studies investigating changes in disorders affecting central respiratory chemoreception

Conclusion

This study characterised the full extent of the adult hRTN using established neurochemical and anatomical markers, locating it to be ventral to 7N, lateral to the superior olive, and overlapped with C1 catecholaminergic neurons. It extends rostrocaudally from Obex +13 mm to Obex +17 mm and comprises 90% of Phox2b+ neurons in the parafacial area, totaling around 5000 bilaterally, being surrounded by numerous TH-ir fibers, and containing an average of 40% of galanin and PACAP. The data herein provides baseline values for future studies looking into clinical contexts such as CCHS and sleep apnea.

Acknowledgements

This work was supported by grants from Australian Research Council (grant no. DP180101890). Tissues were received from the Sydney Brain Bank which is supported by Neuroscience Research Australia and a special gift in memory of Jim Raftos from the Shaw family. We thank Prof Patrice G Guyenet for providing feedback on an advanced version of the manuscript.

References

ABBOTT, S. B., BURKE, P. G. & PILOWSKY, P. M. 2009. Galanin microinjection into the PreBotzinger or the Botzinger Complex terminates central inspiratory activity and reduces responses

to hypoxia and hypercapnia in rat. *Respir Physiol Neurobiol,* 167**,** 299-306.http://dx.doi.org/10.1016/j.resp.2009.06.003
ABERCROMBIE, M. 1946. Estimation of nuclear population from microtome sections. *The Anatomical Record,* 94**,** 239-247.http://dx.doi.org/https://doi.org/10.1002/ar.1090940210
AGOSTINELLI, L. J., MIX, M. R., HEFTI, M. M., SCAMMELL, T. E. & BASSUK, A. G. 2021. Input-output connections of LJA5 prodynorphin neurons. *J Comp Neurol,* 529**,** 635-654.http://dx.doi.org/10.1002/cne.24974
AMIEL, J., DUBREUIL, V., RAMANANTSOA, N., FORTIN, G., GALLEGO, J., BRUNET, J. F. & GORIDIS, C. 2009. PHOX2B in respiratory control: lessons from congenital central hypoventilation syndrome and its mouse models. *Respir Physiol Neurobiol,* 168**,** 125-32.http://dx.doi.org/10.1016/j.resp.2009.03.005
ANTIC, N. A., MALOW, B. A., LANGE, N., MCEVOY, R. D., OLSON, A. L., TURKINGTON, P., WINDISCH, W., SAMUELS, M., STEVENS, C. A., BERRY-KRAVIS, E. M. & WEESE-MAYER, D. E. 2006. PHOX2B mutation-confirmed congenital central hypoventilation syndrome: presentation in adulthood. *Am J Respir Crit Care Med,* 174**,** 923-7.http://dx.doi.org/10.1164/rccm.200605-607CR
BANKHEAD, P., LOUGHREY, M. B., FERNANDEZ, J. A., DOMBROWSKI, Y., MCART, D. G., DUNNE, P. D., MCQUAID, S., GRAY, R. T., MURRAY, L. J., COLEMAN, H. G., JAMES, J. A., SALTO-TELLEZ, M. & HAMILTON, P. W. 2017. QuPath: Open source software for digital pathology image analysis. *Sci Rep,* 7**,** 16878.http://dx.doi.org/10.1038/s41598-017-17204-5
BARNETT, W. H., ABDALA, A. P., PATON, J. F., RYBAK, I. A., ZOCCAL, D. B. & MOLKOV, Y. I. 2017. Chemoreception and neuroplasticity in respiratory circuits. *Exp Neurol,* 287**,** 153-164.http://dx.doi.org/10.1016/j.expneurol.2016.05.036
BHAGWANDIN, A., FUXE, K. & MANGER, P. R. 2006. Choline acetyltransferase immunoreactive cortical interneurons do not occur in all rodents: a study of the phylogenetic occurrence of this neural characteristic. *J Chem Neuroanat,* 32**,** 208-16.http://dx.doi.org/10.1016/j.jchemneu.2006.09.004
BOCHORISHVILI, G., STORNETTA, R. L., COATES, M. B. & GUYENET, P. G. 2012. Pre-Bötzinger complex receives glutamatergic innervation from galaninergic and other retrotrapezoid nucleus neurons. *J Comp Neurol,* 520**,** 1047-61.http://dx.doi.org/10.1002/cne.22769
DEGL'INNOCENTI, D., BECATTI, M., PERUZZI, M., FIORILLO, C., RAMAZZOTTI, M., NASSI, N., ARZILLI, C. & PIUMELLI, R. 2018. Systemic oxidative stress in congenital central hypoventilation syndrome. *Eur Respir J,* 52.http://dx.doi.org/10.1183/13993003.01497-2018
DERELI, A. S., BAILEY, E. J. & KUMAR, N. N. 2021. Combining Multiplex Fluorescence in situ Hybridization with Fluorescent Immunohistochemistry on Fresh Frozen or Fixed Mouse Brain Sections. *J Vis Exp*.http://dx.doi.org/10.3791/61709
DERELI, A. S., OH, A. Y. S., MCMULLAN, S. & KUMAR, N. N. 2024. Galaninergic and hypercapnia-activated neuronal projections to the ventral respiratory column. *Brain Struct Funct,* 229**,** 1121-1142.http://dx.doi.org/10.1007/s00429-024-02782-8
DERELI, A. S., YASEEN, Z., CARRIVE, P. & KUMAR, N. N. 2019. Adaptation of Respiratory-Related Brain Regions to Long-Term Hypercapnia: Focus on Neuropeptides in the RTN. *Front Neurosci,* 13**,** 1343.http://dx.doi.org/10.3389/fnins.2019.01343
DUBREUIL, V., RAMANANTSOA, N., TROCHET, D., VAUBOURG, V., AMIEL, J., GALLEGO, J., BRUNET, J. F. & GORIDIS, C. 2008. A human mutation in Phox2b causes lack of CO2 chemosensitivity, fatal central apnea, and specific loss of parafacial neurons. *Proc Natl Acad Sci U S A,* 105**,** 1067-72.http://dx.doi.org/10.1073/pnas.0709115105
DUBREUIL, V., THOBY-BRISSON, M., RALLU, M., PERSSON, K., PATTYN, A., BIRCHMEIER, C., BRUNET, J. F., FORTIN, G. & GORIDIS, C. 2009. Defective respiratory rhythmogenesis and loss of central chemosensitivity in Phox2b mutants targeting retrotrapezoid nucleus neurons. *J Neurosci,* 29**,** 14836-46.http://dx.doi.org/10.1523/JNEUROSCI.2623-09.2009
EICHER, A. K., KECHELE, D. O., SUNDARAM, N., BERNS, H. M., POLING, H. M., HAINES, L. E., SANCHEZ, J. G., KISHIMOTO, K., KRISHNAMURTHY, M., HAN, L., ZORN, A. M., HELMRATH, M. A. & WELLS, J. M. 2022. Functional human gastrointestinal organoids can be engineered from three primary germ layers derived separately from pluripotent stem cells. *Cell Stem Cell,* 29**,** 36-51.e6.http://dx.doi.org/10.1016/j.stem.2021.10.010

FALKENSTETTER, S., LEITNER, J., BRUNNER, S. M., RIEDER, T. N., KOFLER, B. & WEIS, S. 2020. Galanin System in Human Glioma and Pituitary Adenoma. *Front Endocrinol (Lausanne),* 11**,** 155.http://dx.doi.org/10.3389/fendo.2020.00155

GORIDIS, C. & BRUNET, J. F. 2010. Central chemoreception: lessons from mouse and human genetics. *Respir Physiol Neurobiol,* 173**,** 312-21.http://dx.doi.org/10.1016/j.resp.2010.03.014

GUYENET, P. G. & BAYLISS, D. A. 2015. Neural Control of Breathing and CO2 Homeostasis. *Neuron,* 87**,** 946-61.http://dx.doi.org/10.1016/j.neuron.2015.08.001

GUYENET, P. G. & BAYLISS, D. A. 2022. Central respiratory chemoreception. *Handb Clin Neurol,* 188**,** 37-72.http://dx.doi.org/10.1016/b978-0-323-91534-2.00007-2

GUYENET, P. G., STORNETTA, R. L., SOUZA, G., ABBOTT, S. B. G., SHI, Y. & BAYLISS, D. A. 2019. The Retrotrapezoid Nucleus: Central Chemoreceptor and Regulator of Breathing Automaticity. *Trends Neurosci,* 42**,** 807-824.http://dx.doi.org/10.1016/j.tins.2019.09.002

HU, P., MAITA, I., PHAN, M. L., GU, E., KWOK, C., DIETERICH, A., GERGUES, M. M., YOHN, C. N., WANG, Y., ZHOU, J. N., QI, X. R., SWAAB, D. F., PANG, Z. P., LUCASSEN, P. J., ROEPKE, T. A. & SAMUELS, B. A. 2020. Early-life stress alters affective behaviors in adult mice through persistent activation of CRH-BDNF signaling in the oval bed nucleus of the stria terminalis. *Transl Psychiatry,* 10**,** 396.http://dx.doi.org/10.1038/s41398-020-01070-3

HUANG, J., WATERS, K. A. & MACHAALANI, R. 2017. Pituitary adenylate cyclase activating polypeptide (PACAP) and its receptor 1 (PAC1) in the human infant brain and changes in the Sudden Infant Death Syndrome (SIDS). *Neurobiol Dis,* 103**,** 70-77.http://dx.doi.org/10.1016/j.nbd.2017.04.002

IKEDA, K., KAWAKAMI, K., ONIMARU, H., OKADA, Y., YOKOTA, S., KOSHIYA, N., OKU, Y., IIZUKA, M. & KOIZUMI, H. 2017. The respiratory control mechanisms in the brainstem and spinal cord: integrative views of the neuroanatomy and neurophysiology. *J Physiol Sci,* 67**,** 45-62.http://dx.doi.org/10.1007/s12576-016-0475-y

KASI, A. S., KUN, S. S., KEENS, T. G. & PEREZ, I. A. 2018. Adult With PHOX2B Mutation and Late-Onset Congenital Central Hypoventilation Syndrome. *J Clin Sleep Med,* 14**,** 2079-2081.http://dx.doi.org/10.5664/jcsm.7542

LAVEZZI, A. M., WEESE-MAYER, D. E., YU, M. Y., JENNINGS, L. J., CORNA, M. F., CASALE, V., ONEDA, R. & MATTURRI, L. 2012. Developmental alterations of the respiratory human retrotrapezoid nucleus in sudden unexplained fetal and infant death. *Auton Neurosci,* 170**,** 12-9.http://dx.doi.org/10.1016/j.autneu.2012.06.005

LAZARENKO, R. M., MILNER, T. A., DEPUY, S. D., STORNETTA, R. L., WEST, G. H., KIEVITS, J. A., BAYLISS, D. A. & GUYENET, P. G. 2009. Acid sensitivity and ultrastructure of the retrotrapezoid nucleus in Phox2b-EGFP transgenic mice. *J Comp Neurol,* 517**,** 69-86.http://dx.doi.org/10.1002/cne.22136

LEVY, J., DROZ-BARTHOLET, F., ACHOUR, M., FACCHINETTI, P., PARRATTE, B. & GIULIANO, F. 2021. Parafacial neurons in the human brainstem express specific markers for neurons of the retrotrapezoid nucleus. *J Comp Neurol,* 529**,** 3313-3320.http://dx.doi.org/10.1002/cne.25191

LEVY, J., FACCHINETTI, P., JAN, C., ACHOUR, M., BOUVIER, C., BRUNET, J. F., DELZESCAUX, T. & GIULIANO, F. 2019. Tridimensional mapping of Phox2b expressing neurons in the brainstem of adult Macaca fascicularis and identification of the retrotrapezoid nucleus. *J Comp Neurol,* 527**,** 2875-2884.http://dx.doi.org/10.1002/cne.24713

LITTLE, K., LLORIÁN-SALVADOR, M., TANG, M., DU, X., MARRY, S., CHEN, M. & XU, H. 2020. Macrophage to myofibroblast transition contributes to subretinal fibrosis secondary to neovascular age-related macular degeneration. *J Neuroinflammation,* 17**,** 355.http://dx.doi.org/10.1186/s12974-020-02033-7

MEYLEMANS, A., DEPUYDT, P., DE BAERE, E., HERTEGONNE, K., DEROM, E., DERMAUT, B. & HEMELSOET, D. 2021. Adult-onset congenital central hypoventilation syndrome due to PHOX2B mutation. *Acta Neurol Belg,* 121**,** 23-35.http://dx.doi.org/10.1007/s13760-020-01363-w

MOSTEGL, M. M., RICHTER, B., DINHOPL, N. & WEISSENBÖCK, H. 2011. Influence of prolonged formalin fixation of tissue samples on the sensitivity of chromogenic in situ hybridization. *J Vet Diagn Invest,* 23**,** 1212-6.http://dx.doi.org/10.1177/1040638711425584

MULKEY, D. K. & WENKER, I. C. 2011. Astrocyte chemoreceptors: mechanisms of H+ sensing by astrocytes in the retrotrapezoid nucleus and their possible contribution to respiratory drive. *Exp Physiol*, 96**,** 400-6.http://dx.doi.org/10.1113/expphysiol.2010.053140
OLIVEIRA, L. M., MOREIRA, T. S., KUO, F. S., MULKEY, D. K. & TAKAKURA, A. C. 2016. alpha1- and alpha2-adrenergic receptors in the retrotrapezoid nucleus differentially regulate breathing in anesthetized adult rats. *J Neurophysiol*, 116**,** 1036-48.http://dx.doi.org/10.1152/jn.00023.2016
PATTYN, A., MORIN, X., CREMER, H., GORIDIS, C. & BRUNET, J. F. 1997. Expression and interactions of the two closely related homeobox genes Phox2a and Phox2b during neurogenesis. *Development*, 124**,** 4065-75.http://dx.doi.org/10.1242/dev.124.20.4065
PAXINOS, G., FURLONG, T. & WATSON, C. 2020. *Human brainstem: cytoarchitecture, chemoarchitecture, myeloarchitecture*, Academic Press.
PAXINOS, G., XU-FENG, H., SENGUL, G., & WATSON, C 2012. Organization of brainstem nuclei. In The human nervous system *Elsevier***,** 260-327
PIKKARAINEN, M., MARTIKAINEN, P. & ALAFUZOFF, I. 2010. The Effect of Prolonged Fixation Time on Immunohistochemical Staining of Common Neurodegenerative Disease Markers. *Journal of Neuropathology & Experimental Neurology*, 69**,** 40-52.http://dx.doi.org/10.1097/NEN.0b013e3181c6c13d
RAMIREZ, J. M., SEVERS, L. J., RAMIREZ, S. C. & AGOSTO-MARLIN, I. M. 2018. Advances in cellular and integrative control of oxygen homeostasis within the central nervous system. *J Physiol*, 596**,** 3043-3065.http://dx.doi.org/10.1113/JP275890
ROSIN, D. L., CHANG, D. A. & GUYENET, P. G. 2006. Afferent and efferent connections of the rat retrotrapezoid nucleus. *J Comp Neurol*, 499**,** 64-89.http://dx.doi.org/10.1002/cne.21105
RUDZINSKI, E. & KAPUR, R. P. 2010. PHOX2B immunolocalization of the candidate human retrotrapezoid nucleus. *Pediatr Dev Pathol*, 13**,** 291-9.http://dx.doi.org/10.2350/09-07-0682-OA.1
RYTEL, L., KÖNYVES, L. & GONKOWSKI, S. 2022. Endocrine Disruptor Bisphenol a Affects the Neurochemical Profile of Nerve Fibers in the Aortic Arch Wall in the Domestic Pig. *Int J Environ Res Public Health*, 19.http://dx.doi.org/10.3390/ijerph19105964
SHI, Y., STORNETTA, D. S., REKLOW, R. J., SAHU, A., WABARA, Y., NGUYEN, A., LI, K., ZHANG, Y., PEREZ-REYES, E., ROSS, R. A., LOWELL, B. B., STORNETTA, R. L., FUNK, G. D., GUYENET, P. G. & BAYLISS, D. A. 2021. A brainstem peptide system activated at birth protects postnatal breathing. *Nature*, 589**,** 426-430.http://dx.doi.org/10.1038/s41586-020-2991-4
SHI, Y., STORNETTA, R. L., STORNETTA, D. S., ONENGUT-GUMUSCU, S., FARBER, E. A., TURNER, S. D., GUYENET, P. G. & BAYLISS, D. A. 2017. Neuromedin B Expression Defines the Mouse Retrotrapezoid Nucleus. *J Neurosci*, 37**,** 11744-11757.http://dx.doi.org/10.1523/JNEUROSCI.2055-17.2017
SOUZA, G., STORNETTA, R. L., STORNETTA, D. S., ABBOTT, S. B. G. & GUYENET, P. G. 2020. Differential Contribution of the Retrotrapezoid Nucleus and C1 Neurons to Active Expiration and Arousal in Rats. *J Neurosci*, 40**,** 8683-8697.http://dx.doi.org/10.1523/jneurosci.1006-20.2020
SRINIVASAN, S., DI LUCA, A., ÁLVAREZ, D., JOHN PETER, A. T., GEHIN, C., LONE, M. A., HORNEMANN, T., D'ANGELO, G. & VANNI, S. 2024. The conformational plasticity of structurally unrelated lipid transport proteins correlates with their mode of action. *PLoS Biol*, 22**,** e3002737.http://dx.doi.org/10.1371/journal.pbio.3002737
STORNETTA, R. L., SPIROVSKI, D., MOREIRA, T. S., TAKAKURA, A. C., WEST, G. H., GWILT, J. M., PILOWSKY, P. M. & GUYENET, P. G. 2009. Galanin is a selective marker of the retrotrapezoid nucleus in rats. *J Comp Neurol*, 512**,** 373-83.http://dx.doi.org/10.1002/cne.21897
TAKAKURA, A. C., MOREIRA, T. S., STORNETTA, R. L., WEST, G. H., GWILT, J. M. & GUYENET, P. G. 2008. Selective lesion of retrotrapezoid Phox2b-expressing neurons raises the apnoeic threshold in rats. *J Physiol*, 586**,** 2975-91.http://dx.doi.org/10.1113/jphysiol.2008.153163
WANG, S., SHI, Y., SHU, S., GUYENET, P. G. & BAYLISS, D. A. 2013. Phox2b-expressing retrotrapezoid neurons are intrinsically responsive to H+ and CO2. *J Neurosci*, 33**,** 7756-61.http://dx.doi.org/10.1523/JNEUROSCI.5550-12.2013
WILLIAMS, V. M., BHAGWANDIN, A., SWIEGERS, J., BERTELSEN, M. F., HÅRD, T., SHERWOOD, C. C. & MANGER, P. R. 2022. Distribution of cholinergic neurons in the brains of a lar gibbon and a chimpanzee. *Anat Rec (Hoboken)*, 305**,** 1516-1535.http://dx.doi.org/10.1002/ar.24844

ZHU, M. Y., WANG, W. P., IYO, A. H., ORDWAY, G. A. & KIM, K. S. 2005. Age-associated changes in mRNA levels of Phox2, norepinephrine transporter and dopamine β-hydroxylase in the locus coeruleus and adrenal glands of rats. *Journal of Neurochemistry*, 94**,** 828-838.http://dx.doi.org/10.1111/j.1471-4159.2005.03245.x

Statements & Declarations

Funding

This work was supported by Australian Research Council (Grant number DP180101890, NNK), Research Training Program Domestic Fee Offset (RSAI8000, YL) and Research Training Program Domestic Stipend (RSAP1000, YL).

Competing Interests

The authors do not have relevant financial or non-financial interests to disclose.

Author Contributions

This study was designed by Yazhou Liu, Dr Claire Shepherd, Associate Professor Rita Machalaani and Dr Natasha N Kumar. Irit Markus trained Yazhou Liu in tissue preparation and immunohistochemistry on FFPE tissues. All authors contributed to the methodology validation and experiment troubleshooting. The tissue preparation, experiments, data collection, data analysis and first manuscript draft were produced by Yazhou Liu. Dr Claire Shepherd, Associate Professor Rita Machalaani and Dr Natasha N Kumar revised and modified manuscript drafts.

Data Availability

The datasets generated during during the current study are not publicly available but are available from the corresponding author on reasonable request.

Ethics approval

All donors have previously been collected by the Sydney Brain Bank under UNSW ethics project no. HC#200026. This research project (Project no. HC#200901) was approved by the Human Research Ethics Advisory Panel of the University of New South Wales.

Consent to participate

Informed consent was obtained from the individual participants included in the study prior to tissue donation.

Consent to publish

The authors affirm that human research participants provided informed consent for use of their data for publication.

Figure legend

Figure 1. Adult human brainstem tissue sectioning and RTN region localisation (a) Sagittal schematic of the adult human brainstem and thalamus indicating the angle of tissue sectioning and location spanning from Obex (indicated by blue arrow) +12 mm to +18 mm (between red lines). (b & c) Exemplary brainstem schematics containing the RTN overlaid with H&E stained caudal (Obex +14 mm) and rostral (Obex +16 mm) hemi-sections. (b) Caudally, the RTN (red contour) is encapsulated by a region medial to sp5 and Sp5O, ventral to 7N, lateral to the SO and overlapping with C1 neurons (magenta contour). (c) Rostrally, the RTN region is medial to 7n, ventral to 7N, lateral to MSO and partially overlapping with C1 neurons. Adapted from Paxinos' Human Brainstem Atlas (Paxinos et al., 2020).

Figure 2. Exemplary H&E and primary antibody staining. (a) H&E staining was performed to identify 7N neurons, based on their anatomical location. (b) ChAT immunoreactive cytoplasm and fibers in motor neurons within the 7N. (c) TH immunoreactive cytoplasm and fibers in catecholaminergic C1 neurons. (d) Phox2b immunoreactive nuclei in NTS neurons. (e) PACAP immunoreactive cytoplasm and fibers of hematoxylin counterstained NTS neurons. (f) Galanin-immunoreactive cytoplasm and fibers in the NTS. Arrowheads indicate positive staining.

Figure 3. RTN neurochemical signature and spatial relationship to 7N and C1. a-e: (a) Low power image illustrating the location of the RTN (red contour), C1 region (magenta contour), Sp5O (black contour) and 7N (green contour) in the brainstem. (b) Double immunohistochemical staining for Phox2b and TH demonstrated RTN neurons as Phox2b+ with nuclear localisation (arrowhead), and TH- cytoplasm, which distinguished RTN neurons from C1 neurons. TH immunoreactive fibers (arrowheads) were abundant in the RTN region and closely apposed Phox2b immunoreactive neurons (asterisks). (c) Sp5O neurons exhibited Phox2b immunoreactivity (arrowhead). (d) A few sparsely distributed Phox2b+/TH- neurons were detected dorsomedial to the 7N (arrowhead). (e) C1 neurons (arrowhead) exhibited TH immunoreactivity in the cell cytoplasm and processes and were distributed throughout the RTN region. (f) Low power image illustrating the location of the RTN (red contour) ventral to the 7N (green contour) in the brainstem (Obex +15 mm). (g) Phox2b and ChAT double staining demonstrate RTN neurons as Phox2b+ and ChAT- with nuclear localisation (g, arrowheads). In contrast, the 7N neurons (asterisk) were identified by their ChAT+ soma and relatively large diameter.

Figure 4. Galanin and PACAP immunoreactivities are detectable in large subsets of Phox2b+ parafacial neurons. (a and d) Low magnification image of the RTN region immediately ventral to the 7N. (b) Many neurons in the parafacial region are both galaninergic (brown cytoplasmic labelling) and Phox2b+ (black nucleus staining). (c) Magnification of inset in b) demonstrating a galanin+/Phox2b+ neuron (arrow) and a galanin-/Phox2b+ neuron (arrowhead). (e) A subgroup of

neurons in the parafacial region display PACAP immunoreactivity (brown cytoplasmic labelling) and Phox2b+ (black nucleus staining). (f) Magnification of inset in (e) demonstrating PACAP+/Phox2b+ neuron (arrow) and PACAP-/Phox2b+ neurons (arrowheads).

Figure 5. Schematic coronal hemi-sections illustrating the distribution of Phox2b+/TH- neurons within the parafacial region, representative of the RTN (from Obex +13 mm to Obex +17 mm). Red dots represent Phox2b+/TH- neurons. RTN neurons are located immediately ventral to the 7N, lateral to the SO, and medial to the facial nerve (rostrally) or spinal trigeminal nucleus (caudally). The most densely packed cluster of RTN neurons is situated at 14 mm rostral to Obex. Drawings were made with reference to Paxinos' Human Brainstem Atlas (Paxinos et al., 2020).

Figure 6. RTN neurons extend along the entire rostrocaudal length of the 7N. (a1 and a2) Caudal pole of the 7N (Obex +13.1 mm). (a3) TH+ C1 neuron (asterisk) next to an RTN neuron (arrowhead). (b1 and b2) 7N neurons are distinguished from the RTN region by the green dashed contour. (b3) Many RTN neurons (Phox2b+/TH-, arrowheads) situated ventral to the 7N and TH+ fibers (brown puncata) were particularly dense at this level of the RTN. (c1 and c2) Rostral pole of the 7N (Obex +16.8 mm). (c3) Few RTN neurons (Phox2b+/TH-, arrowhead) were present. A TH+ C1 neuron (asterisk) is visible in the RTN region.

Figure 7. Cell count of the RTN, 7N and C1 neurons. (a) Rostral-caudal distribution and quantification RTN (Phox2b+/TH-) and C1 (Phox2b+/TH+) neurons within the region of interest specified in Fig 2h and Fig 2i. Additionally, total 7N (ChAT+) neurons were counted per hemisection. The rostral-caudal distribution of (b) galaninergic Phox2b+ parafacial neurons and (c) PACAP Phox2b+ parafacial neurons, in the RTN region in two human cases. Data is expressed as the mean ± SEM number of cells/hemi-section.

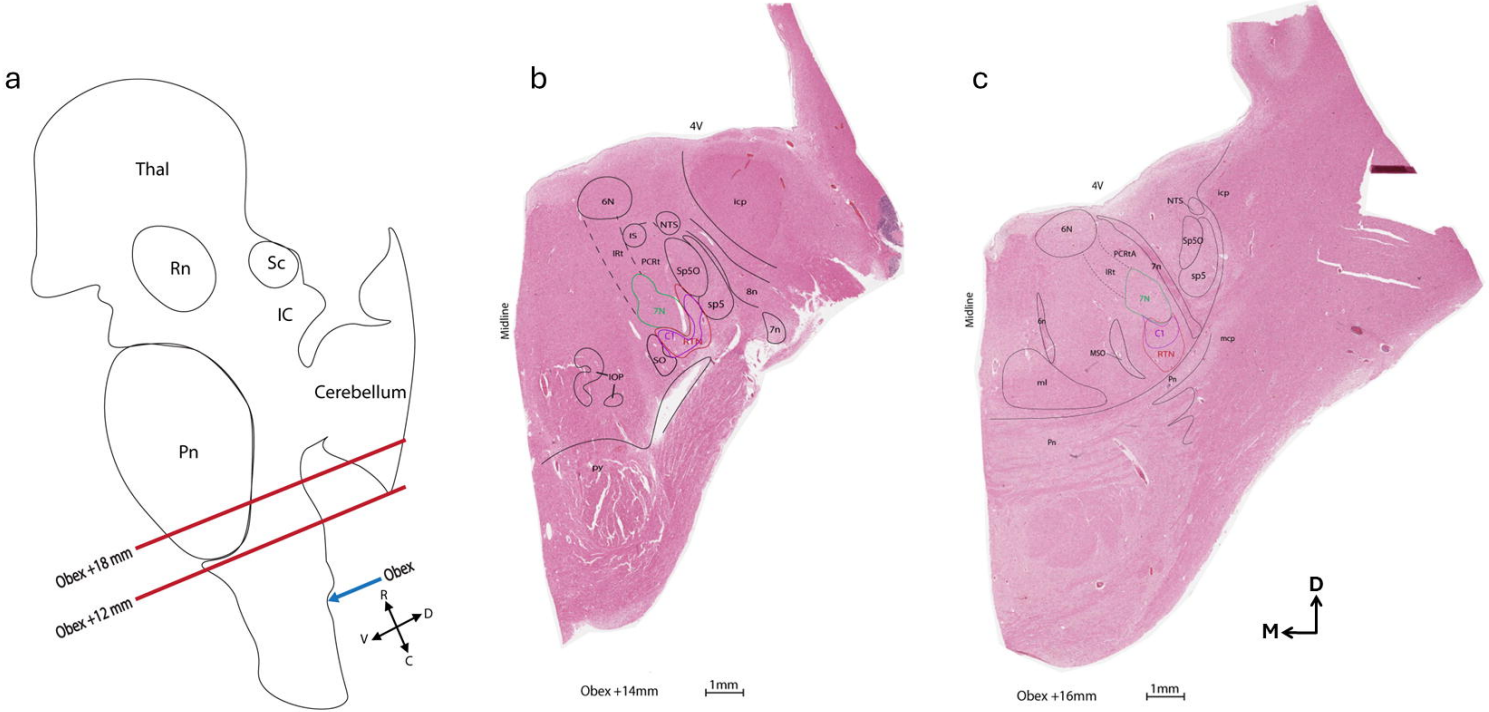
a
Thal
Rn
Sc
IC
Cerebellum
Pn
Obex +18 mm
Obex +12 mm
Obex
R
D
V
C
b
4V
6N
icp
NTS
is
lRt
PCRt
Sp5O
8n
7N
sp5
7n
CT
RTN
SO
IOP
py
Midline
Obex +14mm
1mm
c
4V
NTS
icp
6N
Sp5O
PCRtA
lRt
7n
sp5
7N
6n
CT
mcp
MSO
RTN
ml
Pn
Pn
Midline
D
M
Obex +16mm
1mm

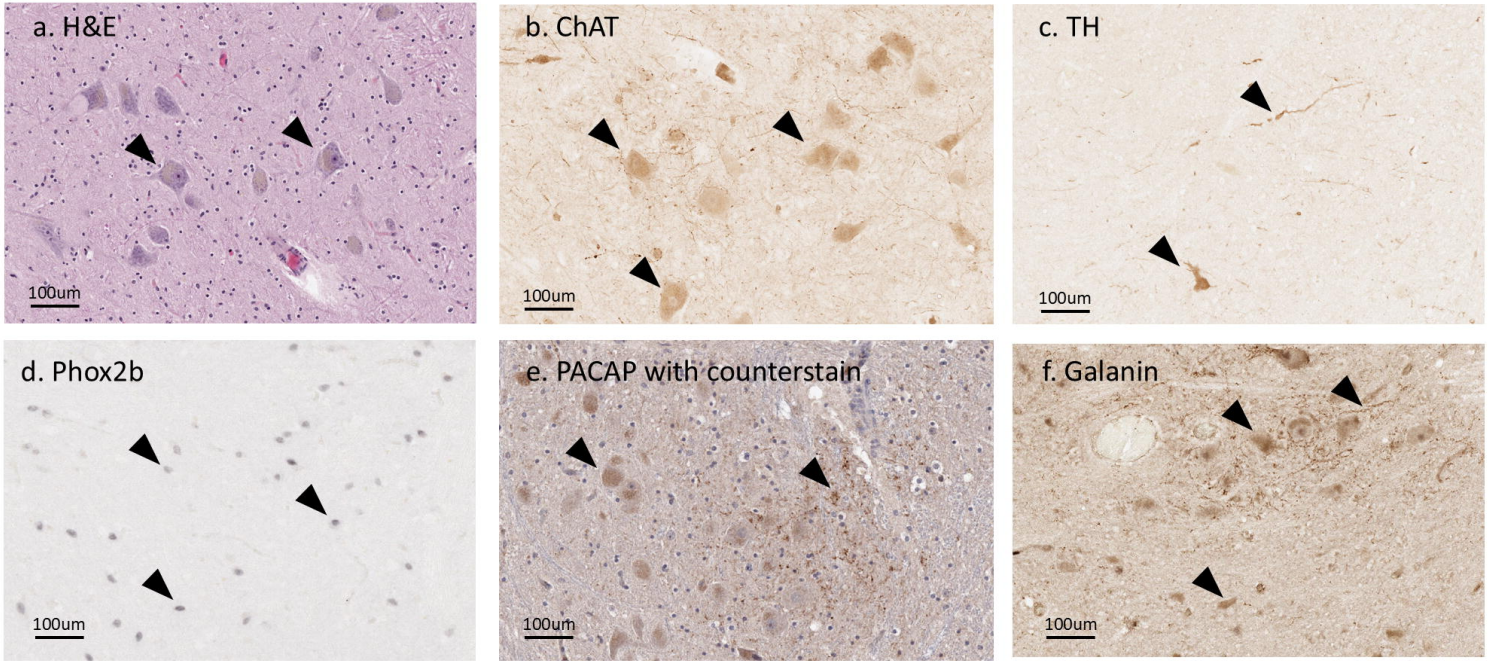
a. H&E
100um
b. ChAT
100um
c. TH
100um
d. Phox2b
100um
e. PACAP with counterstain
100um
f. Galanin
100um

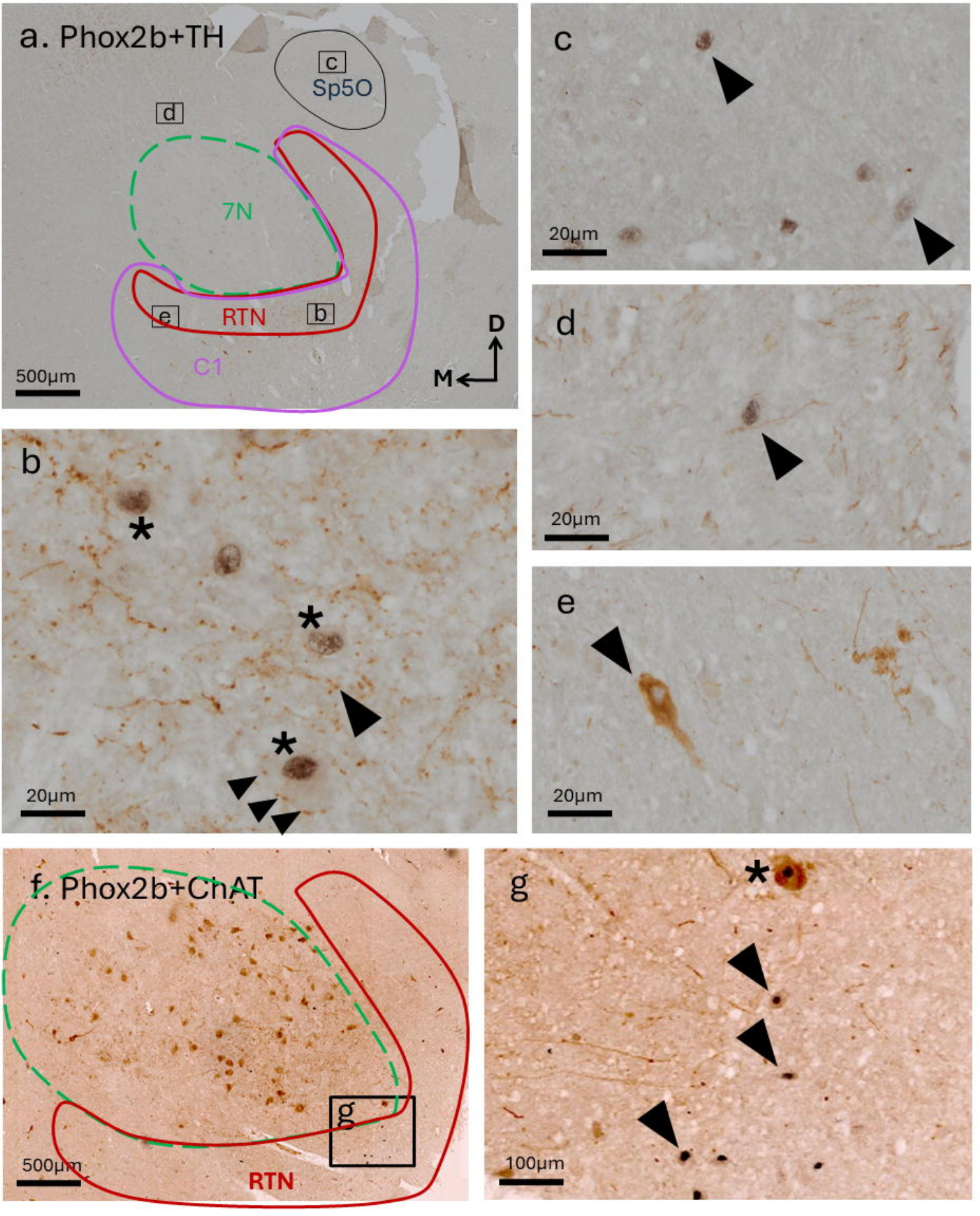
a. Phox2b+TH
c
Sp5O
d
7N
e
RTN
b
C1
D
M
500µm
c
20µm
d
20µm
b
20µm
e
20µm
f. Phox2b+ChAT
g
500µm
RTN
g
100µm

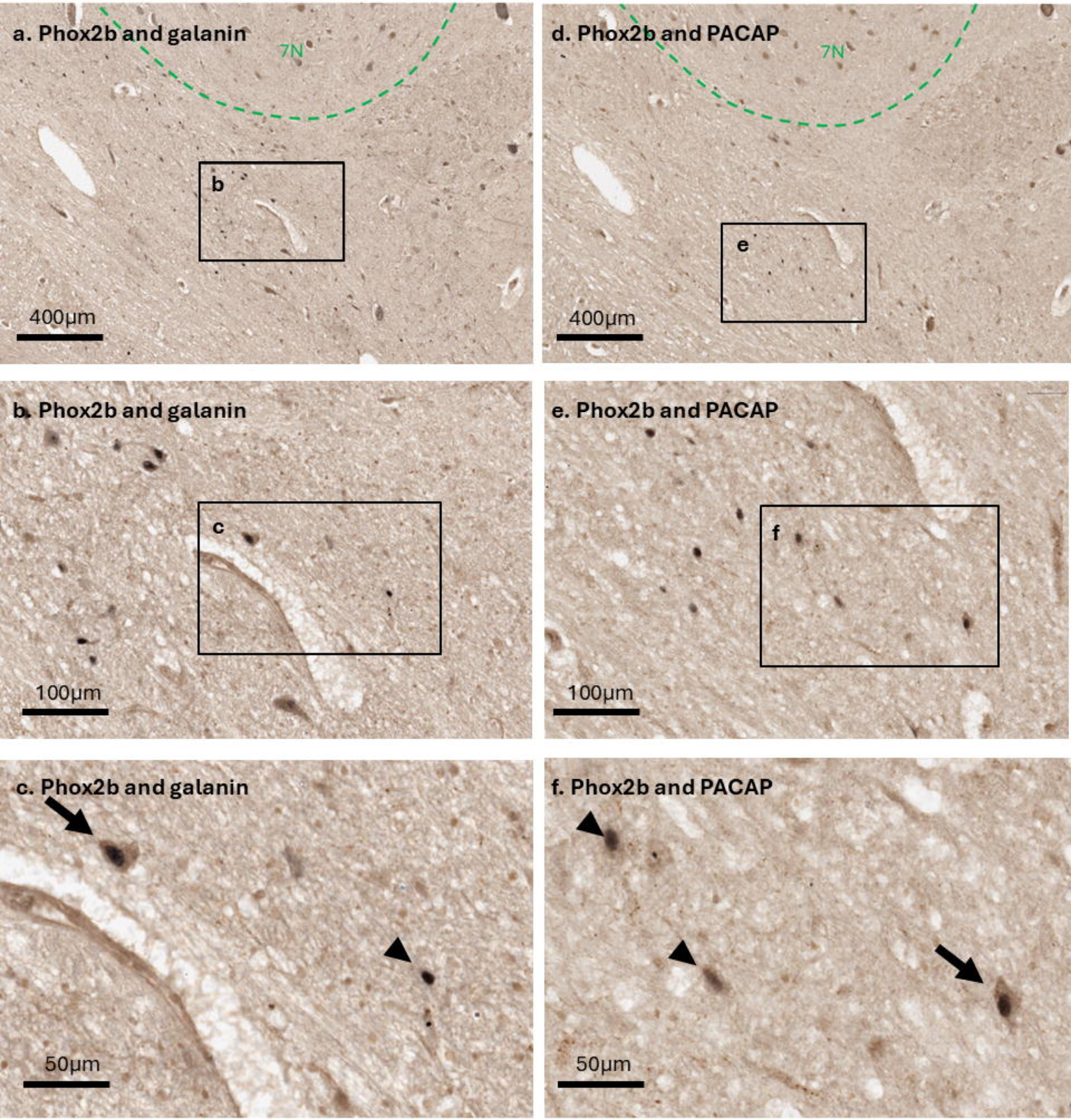
a. Phox2b and galanin
7N
b
400µm
d. Phox2b and PACAP
7N
e
400µm
b. Phox2b and galanin
c
100µm
e. Phox2b and PACAP
f
100µm
c. Phox2b and galanin
50µm
f. Phox2b and PACAP
50µm

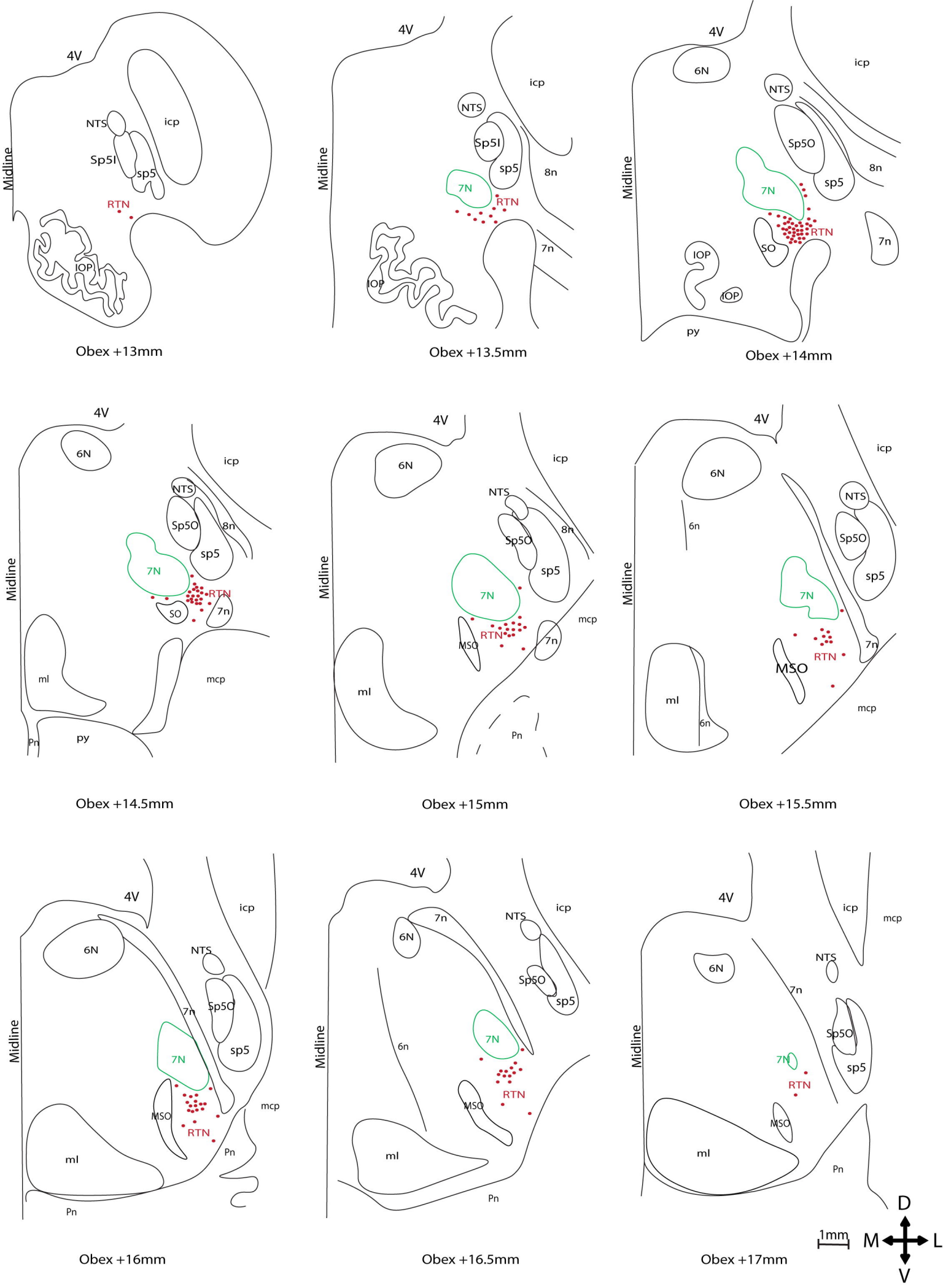
4V
NTS
icp
Sp5I
sp5
RTN
IOP
Midline
Obex +13mm
4V
icp
NTS
Sp5I
sp5
8n
7N
RTN
7n
IOP
Midline
Obex +13.5mm
4V
6N
icp
NTS
Sp5O
8n
sp5
7N
RTN
SO
7n
IOP
IOP
py
Midline
Obex +14mm
4V
6N
icp
NTS
Sp5O
8n
sp5
7N
RTN
SO
7n
ml
mcp
Pn
py
Midline
Obex +14.5mm
4V
6N
icp
NTS
Sp5O
8n
sp5
7N
mcp
RTN
MSO
7n
ml
Pn
Midline
Obex +15mm
4V
icp
6N
NTS
6n
Sp5O
sp5
7N
7n
RTN
MSO
ml
6n
mcp
Midline
Obex +15.5mm
4V
icp
6N
NTS
Sp5O
7n
sp5
7N
mcp
MSO
RTN
ml
Pn
Pn
Midline
Obex +16mm
4V
7n
NTS
icp
6N
Sp5O
sp5
6n
7N
RTN
MSO
ml
Pn
Midline
Obex +16.5mm
4V
icp
mcp
NTS
6N
7n
Sp5O
sp5
7N
RTN
MSO
ml
Pn
Midline
Obex +17mm
1mm
D
M
L
V

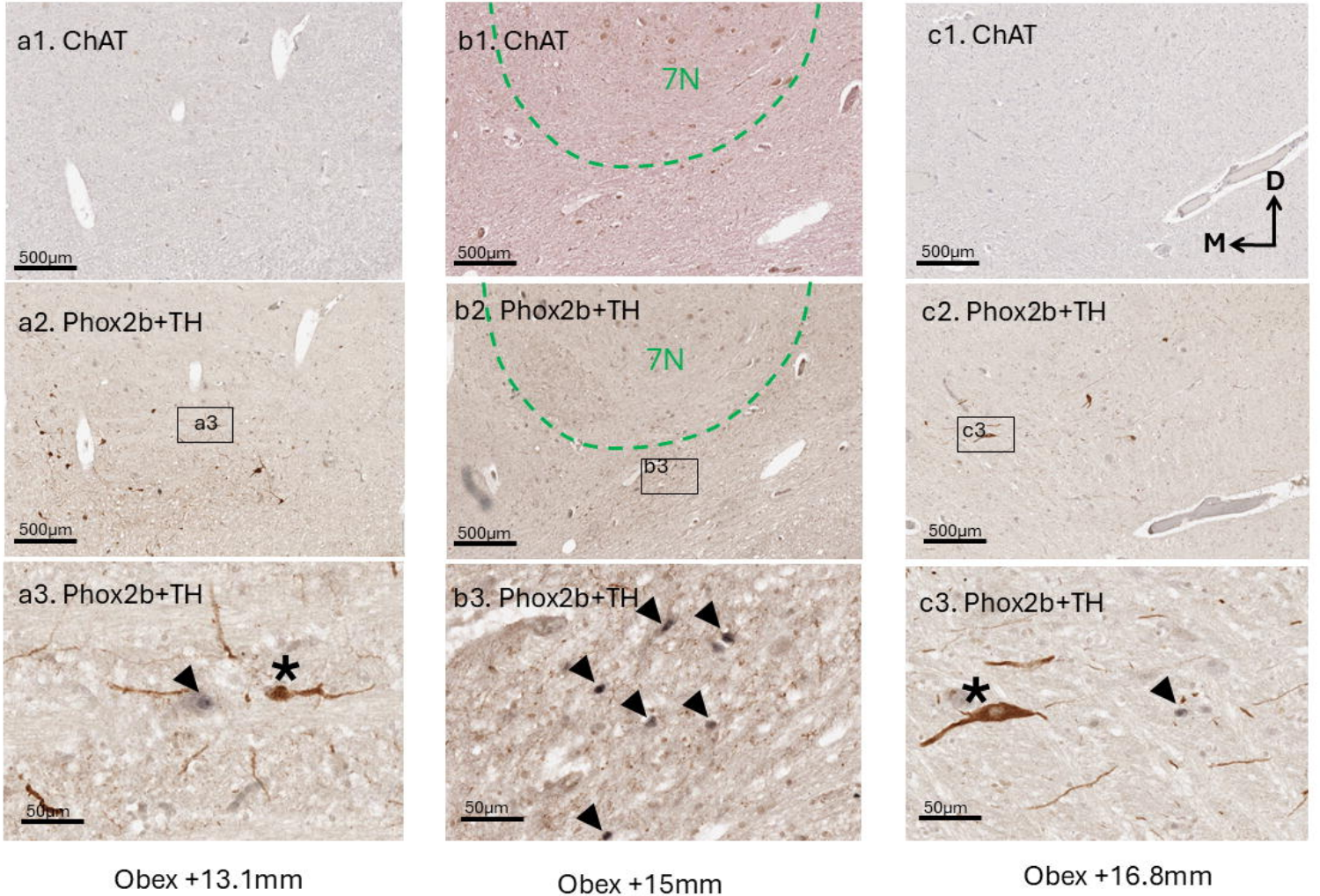
a1. ChAT
500µm
b1. ChAT
7N
500µm
c1. ChAT
D
M
500µm
a2. Phox2b+TH
a3
500µm
b2. Phox2b+TH
7N
b3
500µm
c2. Phox2b+TH
c3
500µm
a3. Phox2b+TH
50µm
b3. Phox2b+TH
50µm
c3. Phox2b+TH
50µm
Obex +13.1mm
Obex +15mm
Obex +16.8mm

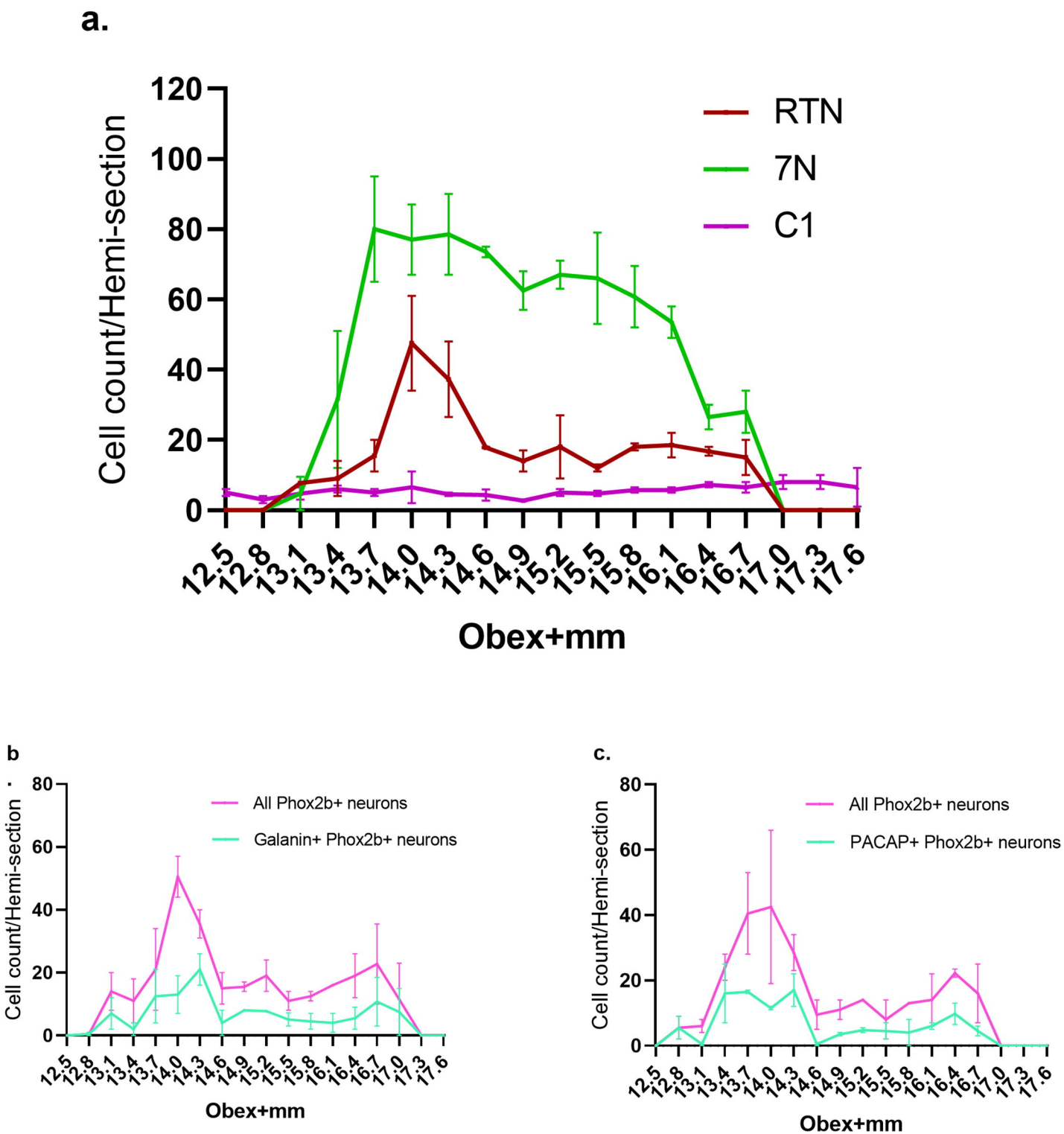
a.
Cell count/Hemi-section
120
100
80
60
40
20
0
RTN
7N
C1
12.5
12.8
13.1
13.4
13.7
14.0
14.3
14.6
14.9
15.2
15.5
15.8
16.1
16.4
16.7
17.0
17.3
17.6
Obex+mm
b
Cell count/Hemi-section
80
60
40
20
0
All Phox2b+ neurons
Galanin+ Phox2b+ neurons
Obex+mm
c.
Cell count/Hemi-section
80
60
40
20
0
All Phox2b+ neurons
PACAP+ Phox2b+ neurons
Obex+mm

Table 1: Summary of data collected on primate RTN in chronological order.

Developmental age, number of cases, Sex ratio	**Tissue Frozen or FFPE, and plane of cut (coronal vs sagittal)**	**Sections/case analysed; Obex/bregma level**	**Antibody/probe details & dilution**	**RTN Phox2b subcellular staining pattern & anatomical location**	**Number of RTN neurons (bilateral)**	**Reference**
Human fetuses and infants (19-44w, n=8)	5 µm coronal (n=5) and sagittal (n=3) FFPE sections	1-2 sections/case (level not specified but in the presence of the 7N).	Rabbit anti-PHOX2B (gift of J.-F. Brunet, 1:1000). NK1R (Abcam, 1:200); TH (Chemicon, 1:1000)	IHC: cell nucleus. RTN was ventral to 7N and lateral to the SO in the pontomedullary junction.	Not provided	(Rudzinski and Kapur, 2010)
Human fetuses (35-40w, n=9) and infant (2-8 months, n=11)	4 µm coronal FFPE sections	3-6 sections/case: 1-2 sections from each brainstem level of upper pons, upper medulla and from Obex -2/3 mm to +2/3 mm.	Rabbit anti-PHOX2B (gift of J.-F. Brunet, 1:750)	IHC: cell nucleus and cytoplasm. RTN located between the 7N and SO in caudal pons**.**	980 ±23 Phox2b+ neurons However, equation applied not provided	(Lavezzi et al., 2012)
Macaca fascicularis (5- & 6-years old males and 16-year-old female, n=2 IHC; n=1 ISH)	40 µm coronal frozen and paraformaldehyde fixed free-floating sections	60 sections/case (1/8 serial sections); Obex -1.40mm to +13mm.	IHC: Rabbit anti-Phox2b antibody (1:2,000; gift from J-F. Brunet) ISH: ppGal and Phox2b mRNAs	IHC: subcellular location of staining not described. Parafacial region located ventral and lateral to 7N; ISH: cell cytoplasm. ppGal+/Phox2b+ RTN neurons located caudal,	2400 ppGal+/Phox2b+ neurons. ppGal-/Phox2b neurons were not included. Calculated as an estimation by automated method yet cautions on possibility of double counting.	(Levy et al., 2019)

				ventral and lateral to 7N spanning from Obex +4.56 mm to +10.16 mm.		
Human adults (n=2)	10 µm coronal FFPE sections	60 sections/case (1/10 serial sections), Obex +14 mm to +17 mm.	mRNA probes (targeting 237–492 sequence of the galanin message-associated peptide mRNA (i.e. ppGal) and 469–1173 sequence of the vGlut2 mRNA (SLC17A6) and NMB.	IHC: N/A since Phox2b did not work. ISH: N/A since Phox2b did not work. Based on ppGal, SLC17A6 and NMB, RTN located in parafacial region.	Not provided	(Levy et al., 2021)
Human adults (n=2)	10 µm coronal FFPE sections	90 sections/case (5/30 serial sections), Obex +12 mm to +18 mm.	Mouse anti-Phox2b (Bio-Strategy Laboratory, cat#sc-376997, 1:1000)	IHC: cell nucleus RTN was identified ventral to 7N, lateral to the SO and medial to facial nerve and Sp5O.	Approximately 5000 Phox2b+TH-ChAT-RTN neurons.	Study herein

Phox2b rabbit polyclonal antibody was raised against the 14 amino-acid C-terminal sequence of the Phox2b protein, with the addition of a tyrosine at the N-terminal end (YFHRKPGPALKTNLF; (Pattyn et al., 1997)). ^ raised against amino acids 11-70 mapping near the N-terminus of Phox2b of human origin

Table 2. Primary and secondary antibodies used for immunohistochemistry (IHC)

Antibody	Source (Catalogue Number), RRID	Immunogen	Validation	Target & expected subcellular staining	Dilution
Primary (1º) Antibodies					
Mouse monoclonal anti-Phox2b IgG antibody	Bio-Strategy Laboratory (sc-376997), RRID: AB_2813765	Human origin N-term amino acids 11-70	IHC: cross-reactivity with mouse brain tissue ISH: co-localisation with Phox2b mRNA labelled using RNAscope (Dereli et al., 2021)	Phox2b transcription factor (e.g. nucleus of RTN and C1 neurons)	1:1000
Chicken anti-Tyrosine Hydroxylase (TH)	Aves Labs (TYH-0020), RRID: AB_10013440	Human tyrosine hydroxylase (E.C.1.14.16.2) protein	IF: human gastric tissue (Eicher et al., 2022).	Catecholaminergic neurons (e.g. cytoplasm of C1 neurons)	1:6000
Goat anti-Choline Acetyltransferase (ChAT)	Millipore Sigma (AB144P), RRID: RRID AB_2079751	Human placental enzyme	IHC: rat brain tissue (1:200) (Bhagwandin et al., 2006); IHC: ape brain tissue (1:3000) (Williams et al., 2022)	Cholinergic neurons (e.g. cytoplasm of 7N)	1:1000
Rabbit anti-Galanin	Peninsula Laboratories International (T-4325), RRID: not provided	Synthetic peptide H-Gly-Trp-Thr-Leu-Asn-Ser-Ala-Gly-Tyr-Leu-Leu-GlyPro-His-Ala-Val-Gly-Asn-His-Arg-Ser-Phe-Ser-Asp-Lys-Asn-Gly-LeuThr-Ser-OH coupled to carrier protein.	IHC: human brain tissue (1:300)(Falkenstetter et al., 2020)	Galaninergic neurons (e.g. cytoplasm of NTS and RTN neurons)	1:300

Rabbit anti-PACAP	Abcam (ab216627), RRID: Not provided	Human ADCYAP1 aa 150 to C-terminus	IF: Pig nerve fibers in the aortic arch wall (1:4000) (Rytel et al., 2022); IHC: mouse brain tissue (1:700) (Hu et al., 2020).	PACAP neuropeptide (e.g. cytoplasm of NTS and RTN neurons)	1:300
Secondary (2º) Antibodies					
Biotin-SP-conjugated Donkey anti-Mouse IgG	Jackson ImmunoResearch (715-035-150), RRID: AB_2340770	Whole molecule mouse IgG	WB: Human HeLa cells (1:10000) (Srinivasan et al., 2024)	Mouse anti-Phox2b 1º Ab	1:500
Biotin-SP-conjugated Donkey anti-Chicken IgG	Jackson ImmunoResearch (703-065-155), RRID: AB_2313595	Whole molecule chicken IgY	IHC: mouse eyes (dilution not provided) (Little et al., 2020)	Chicken anti-TH 1º Ab	1:500
Biotin-SP-conjugated Donkey anti-Goat IgG	Jackson ImmunoResearch (705-065-147), RRID: AB_2340397	Whole molecule goat IgY	IHC: Mouse brain and spine tissue (1:500) (Agostinelli et al., 2021)	Goat anti-ChAT 1º Ab	1:500
Biotin-SP-conjugated Donkey anti-Rabbit IgG	Jackson ImmunoResearch (711-065-152), RRID: AB_2340593	Whole molecule rabbit IgY	WB: Human HeLa cells (1:10000) (Srinivasan et al., 2024)	Rabbit anti-PACAP 1º Ab	1:500

Table 3. The morphological characteristics based on the respective subcellular neurochemical signature of the RTN, 7N and C1 neurons

Cell Type	Morphology	Nucleus: Area (μm^2)	Cell Area (μm^2)	Cell Diameter (µm)	subcellular neurochemical profile		
					Cytoplasm	Nucleus	Axon
7N neurons (n=68, 1 section/case)	Large multipolar neurons with short dendrites	274.6± 108.0	1194.0± 371.8	41.8±10.7	ChAT+, TH-, PACAP+/-, galanin-	Phox2b+/-	ChAT+
RTN neurons (n=241, 3 sections/case)	Medium round or fusiform neurons with short dendrites	69.0± 23.3	309.9± 61.8	19.9±4.0	ChAT-, TH-, PACAP+/-, Galanin+/-	Phox2b+	undetected
C1 neurons (n=50, 4 sections/case)	Medium multipolar neuron with short dendrites and long projecting axons	108.3± 46.3	539.0± 226.8	34.6±10.0	ChAT-, TH+, PACAP+/-, galanin-	Phox2b+/-	TH+

Mean ± standard deviation.

Table 4. Total Phox2b+ parafacial neurons and the proportion that are galanin+ or PACAP+*

	Phox2b+ RTN neurons*	**Phox2b+ parafacial neurons**	**Phox2b+/ PACAP+ parafacial neurons**	**Phox2b+/galanin+ parafacial neurons**	**% of Phox2b+ parafacial PACAP+ neurons**	**% of Phox2b+ of parafacial galanin+ neurons**
Case 1	5300	5960	2420	2985	41	50
Case 2	4903	4630	1760	1540	38	33
Average	5102	5295	2090	2262	39	43

*please refer to Supplement Table 3 which shows the breakdown of the counts according to intensity of staining.